Surface functionalization strategy to enhance the antibacterial effect of nisin Z peptide

Pascal Thébault[*1], *Mohamad Ammoun*[2], *Rym Boudjemaa*[2], *Aimeric Ouvrard*[2], *Karine Steenkeste*[2], *Bernard Bourguignon*[2], *Marie-Pierre Fontaine-Aupart*[2]

[1] Normandie Univ, UNIROUEN, INSA Rouen, CNRS, PBS, 76000, Rouen, France

[2] Université Paris-Saclay, CNRS, Institut des Sciences Moléculaires d'Orsay, 91405, Orsay, France

KEYWORDS: *Antimicrobial peptides, antibacterial surfaces, XPS, FITR-ATR spectroscopy, SHG, confocal microscopy*

ABSTRACT

One of the main challenges when building antibacterial surfaces with antimicrobial peptides (AMPs) is to preserve their antimicrobial activity after stable immobilization of the peptides. Among all parameters, order/conformation of self-assembled monolayers, used as spacer, is one the most important. Herein we report the covalent immobilization of the nisin Z peptide on a gold surface functionalized with a self-assembled monolayer of 11-mercaptoundecanoic acid (MUA) alone or mixed with 6-mercaptohexanol, used as a spacer. The MUA acid is activated by treatment with carbodiimide/N-hydroxysuccinimidine and then reacts with nisin Z to form amide bonds via the N terminal part of the peptide. We have characterized each step of the surface modification using X-ray photoelectron spectroscopy, FTIR-ATR spectroscopy and contact angle measurements. The combined results show the success of each functionalization step. Additionally, SFG brings information on the orientation and conformational ordering of the self-assembled monolayers. Indeed, a better order of MUA25 layers compared to MUA was observed due to the spacing of carboxylic acid groups. The antibacterial activity of the immobilized AMPs against *Staphylococcus aureus* is evaluated using confocal microscopy and bacterial counting: it increases with a better order of the SAMs rather than a greater peptide concentration. This study provides fundamental insights on how to engineer AMPs and substrate to produce efficient biocidal surfaces.

INTRODUCTION

The colonization of abiotic surfaces by bacteria (microbial contamination) is a real plague for public health (nosocomial infections, chronic wounds, rejection of implants ...), food industry

(alterations and poisoning of foodstuffs), cosmetics (product degradation causing skin problems for the consumer) or industrial sector (biocorrosion phenomena, occlusions of cooling circuits ...) (1).

It is now accepted that for any microorganism, life in a fixed form (called sessile) is favored over a suspended lifestyle (called planktonic). In most cases, this results in the formation of a biofilm that allows the bacteria to persist and even to resist in an unfavorable environment (2). This "way of life" (sessile state) has been shown to make bacteria up to 1000 times less sensitive to antibiotic or other bactericidal treatments than their planktonic counterparts (3), making the fight against bacterial contamination of surfaces very problematic. In this context, prevention seems preferable to any treatment. The best approach may rely on new surface coatings that resist or prevent adhesion of bacteria and/or their growth to form biofilms.

Bacterial adhesion on surfaces strongly depends on the physico-chemical properties of both the microorganisms and the substrate. The surface of bacteria are amphiphilic while they are globally negatively charged. Therefore a common approach relies on the development of highly hydrophobic or negatively charged surfaces to preclude the adhesion of bacteria and /or their growth (4–6). However, microorganisms will inevitably adhere to some extent to these coatings due in particular to the micro-heterogeneity of positive charges on the bacteria surface (7) and surprisingly, despite a slower initial adhesion, surface growth of the adhering bacteria may be higher (8). Another strategy is the immobilization of active biocides (quaternary ammoniums, antibiotics, metal salts, metallic nanoparticles…) on the surfaces to promote bacterial killing (9,10). This approach also presents some drawbacks, especially because antibacterial agents with high potential toxicity can be released and contribute to environmental pollution and to the emergence of multi-resistant bacterial strains. Such a situation has required to consider new biocidal candidates displaying anti-adhesive and/or antibacterial properties with low toxicity as well as surface coating strategies for long term biocidal stability.

In this sense, developing surfaces using a covalent binding process of antimicrobial peptides (AMPs) appears very attractive (11–17). Compared to antibiotics, some AMPs offer the advantages of having a broad spectrum of activity, of not promoting bacterial resistance and of being active at very low concentrations (10,18). Otherwise, covalent immobilization of AMPs is reported to limit their release, which avoids the drawbacks mentioned above.

We are interested in developing such biocidal surfaces against *Staphylococcus aureus*, one of the most frequent agents of biofilm-related infections in medical and food environments and one of the most critical multidrug-resistant bacteria (19). In this context, the covalent immobilization of the AMP nisin Z onto surfaces may be a promising strategy to create

materials with friendly environmental and health impact. nisin Z, produced by Lactic acid bacteria, is the only one peptide recognized as safe by the U.S. Food and Drug Administration (20). Its antimicrobial activity in the nanomolar-range, its lack of toxicity for humans and its resistance to thermal treatments lead to its massive use in food industry as a preservative against Gram-positive bacteria including *S. aureus* (10,21).

Reported studies have highlighted that the antimicrobial activity of covalently immobilized AMPs onto surfaces is generally lower than that of their soluble counterparts (10). It can be due, to the impossibility for immobilized AMPs to cover all the surface of the target bacteria as in solution, but only one side of the cell, limiting the multiple interactions with the bacteria cell wall surface. The peptide mode of action of the AMP must also be considered. Typically nisin Z can bind lipid II with high affinity to form pores in the cytoplasmic membrane of target cells and also block peptidoglycan biosynthesis, thus inhibiting cell-wall formation (22). According to this mode of action, one could expect that the immobilized nisin Z peptides would lose their antibacterial activity against Gram positive bacteria having peptidoglycane cell wall above the cytoplasmic membrane. Indeed, the length of the immobilized peptide standing up on the surface is ~ 40-50 Å (33 peptidic bonds), ten times too short to allow the peptide to penetrate the cell wall of *S. aureus* bacteria (of thickness ~40 nm) (23). The activity of the immobilized peptides also strongly depends on several parameters of the functionalized surfaces (peptide surface density, length and flexibility of the spacer that binds the AMP to the surface, etc..), all these requiring to be mastered for a better control of surface chemistry and topography.

In this study, we are interested to decipher the role of self-assembled monolayers orientation used as spacer on the activity of immobilized nisin Z. This point has not been systematically addressed because it requires nanoscopic specific method such as sum frequency generation (SFG) vibrational spectroscopy, a nonlinear optical technique that is interfaced specific. The method was used to characterize two different self-assembled monolayers (SAMs) of 11-mercaptoundecanoic acid (MUA) alone or mixed with 6-mercaptohexanol, to covalently immobilize the nisin Z peptide on a gold model surface. Then the antibacterial efficiency of these AMP surfaces against *S. aureus* was evaluated through fluorescence confocal microscopy and bacteria counts.

Experimental section

Materials

Mercaptoundecanoic acid (MUA, $C_{11}H_{22}O_2S$), 6-mercaptohexanol (C_6OH), N-hydrosuccinimide (NHS), absolute ethanol, 1-ethyl-3-(3-dimethylaminopropyl) carbodiimide hydrochloride (EDC), Hydrochloric acid (HCl) and Phosphate buffer saline (PBS) tablets were purchased from Sigma-Aldrich. Nisin Z was purchased from Anhui mimetals development (China). It was chosen because it is the only AMP authorized by the FDA and the WHO. nisin Z is a cyclic antibiotic of 34 amino acids (20,24–26), largely randomly coiled in aqueous solution (27). It differs from nisin A by the replacement of a histidine by an asparagine residue at position 27. Because nisin Z contains only one histidine residue, it has a higher solubility at physiological pH (the pKa of His being ~6.5 in water). The stock solutions were prepared at 10 mg/ml in HCl 0,0001N. The gold surfaces (11x11 mm size, purchased from Arrandee (Germany)) are borosilicate glass substrates coated with layers of chromium and gold of thicknesses 2.5 ± 1.5 nm and 250 ± 50 nm respectively. The surfaces were annealed in a butane flame to ensure a good crystallinity of the topmost layers, rinsed in a bath of absolute ethanol during 10 min and then dried under a flow of dry nitrogen before use.

Surface preparation and characterization

Cleaned gold surfaces were immersed in absolute ethanol containing MUA (10 mM) or a binary mixture (25/75) of MUA (2.5 mM) and 6-mercaptohexanol ($HS(CH_2)_6$ OH) (7.5 mM). These substrates named Au-MUA and Au-MUA25 respectively were then (i) stirred on an orbital shaker during 3 h in order to ensure optimal homogeneity of the adlayer and (ii) thoroughly rinsed successively in an absolute ethanol and milliQ water baths on an orbital shaker during 10 min before (iii) drying under a flow of dry nitrogen.

The functionalized surfaces were then immersed in a solution of EDC/NHS (10/20 mM) in milliQ water for 90 min at room temperature (Au-MUA_{act} and Au-MUA25 $_{act}$ surfaces). The resulting succinimidyl ester-terminated surfaces were copiously rinsed in milliQ water baths on an orbital shaker during 10 min and dried under a flow of dry nitrogen. Finally, a 150 µl drop of nisin Z (1 mg/ml in PBS, pH 7.4) was deposited on the activated substrates at room temperature during 2h. This concentration is large enough to ensure the grafting of at least one peptide by activated MUA chain. The final Au-MUA-Nis and Au-MUA25-Nis substrates were successively rinsed in PBS and milliQ water baths on an orbital shaker during 10 min and dried under a flow of dry nitrogen.

Each step of the process was characterized by a combination of XPS, FTIR-ATR and water-contact angle methods as reported in Supplementary Information.

SFG vibrational spectroscopy

Our home-made "BB"-SFG setup (for Broad Band) was described in details previously (28). It uses tunable IR pulses (4 µJ/pulse, 120 fs pulse duration, and 150 cm^{-1} bandwidth) and "visible" pulses (806 nm, 2 µJ, adjustable duration and bandwidth 1-6 ps ≡ 15-2.5 cm^{-1}, the spectral resolution being determined by the visible laser bandwidth). The two laser beams were superimposed onto the substrates in a collinear co-propagating configuration at the incident angle of ~66° in p polarization. The laser spot size on the sample surface was ~100 µm. After thorough rejection of light from the visible beam by dichroic filters, the beam emitted at the sum frequency was focused on the entrance slit of a spectrometer of resolution 0.4 cm^{-1} centered at ≈650 nm or ≈714 nm for detection of the CH and amide bands respectively, equipped with a cooled CCD camera. The SFG spectra were collected during 30 to 150 seconds to obtain an acceptable signal to noise ratio. SFG vibrational spectra were collected for all substrates in the air. Attempts to obtain SFG signal using s polarization of the visible and IR beams failed.

SFG vibrational spectra were recorded in two different spectral ranges: the 2800-3000 cm^{-1} range for analyzing CH_3 and CH_2 vibrational bands (in this case the IR pulse frequency was set at 2900 cm^{-1}) and the range 1500-1700 cm^{-1} for analyzing amide bands (in this case the IR pulse was set at ≈ 1600 cm^{-1}). In this 1500-1700 cm^{-1} range, absorption by gas-phase water molecules is so strong that the IR laser is almost completely absorbed at the frequencies of the strongest absorption lines. Therefore, the set-up (IR laser cavity and all the optical path to the sample) was purged by dry air one night in advance and the key optical mounts were motorized for last minute adjustments. In addition, an airlock was used for sample introduction allowing to install samples with minimal water vapor contamination. The residual small imprint of the water spectrum on the spectral profile of the IR laser was then easily removed before deconvolution of the vibrational bands against the non-resonant background of the SFG spectrum. The rest of spectral analysis was as described in earlier papers (28).

It must be recalled that there are two major specificities of SFG vibrational spectroscopy with respect to FTIR-ATR spectroscopy (29): (i) the vibrational bands of molecules adsorbed on gold interfere with a non-resonant (NR) background. In BB-SFG configuration, this background has the spectral shape of the IR femtosecond laser (SFG reference spectra in Figure 2). It provides a reference for comparison of intensities from one sample to the other (while absolute intensities of different spectra are difficult to compare because they are strongly dependent on optical alignment). (ii) Due to the coherent nature of SFG emission, the

amplitudes of identical chemical groups sum up instead of intensities, with two possible consequences (both arising in this study): (a) if the orientation distribution of the transition moments of the contributing chemical groups is isotropic, then the intensity vanishes. In such a case, a low intensity means "disorder" in the sense of an isotropic distribution of the different chemical groups. (b) in the case where the sample is highly ordered with a centrosymmetric arrangement of the contributing chemical groups, then the SFG intensity also vanishes. This is typically the case of CH_2 bands of all-trans alkyl chains in SAMs, for which zero intensity means "order" (28).

Antibacterial effect of nisin Z coated surfaces

Staphylococcus aureus ATCC 27217 strain (BioMérieux, France) was used in the present study. After two subcultures in TSB at 37°C (one 8-h followed by an overnight culture of a stock strain culture cryotube kept at -20°C in TSB), cells were harvested by centrifugation, washed twice in sterile NaCl (150 mM) and suspended in TBS. Optical density was measured at 600 nm to control the initial bacterial concentration (~10^8 UFC/ml). The cleaned substrates (Au substrates, Au-MUA and Au-MUA25-without and with nisine Z) were incubated with 500 µl of the bacterial suspension in a static mode over 1h30 at 37°C (in this condition, the *S.aureus* cells could adhere but not grow on the surface). It must be noted that only the functionalized side of the gold-coated surface was accessible for the bacteria to adhere. Before observation, the samples were carefully rinsed to eliminate non-adherent cells (which can be dead cells during time of adhesion) and further recovered with sterile NaCl (150 mM).

The visualization of bacterial adhesion and subsequent cell development on nisin Z functionalized substrates was performed using a Leica TCS SP5 confocal laser scanning microscope (Leica Microsystems, France) at the Centre de Photonique pour la Biologie et les Matériaux (CPBM) (Orsay, France). Bacteria were stained with 2.5 µM Syto9® (Life Technologies, France), a green cell permeant nucleic acid dye, and 30 µM propidium iodide (PI) (Life Technologies, France), a red nucleic acid dye that can easily penetrate cells with compromised plasma membranes. Syto9® and PI were sequentially excited at 488 nm and 543 nm, respectively, and their fluorescence emissions were collected between 500 and 600 nm for Syto9® and between 640 and 750 nm for PI. Images were acquired using a 63x oil immersion objective with a 1.4 numerical aperture. The size of the confocal images was 512 by 512 pixels corresponding to image sizes of 246 x 246 μm^2 for zoom 1 and 82 x 82 μm^2 for zoom 3. For each sample, 5 different areas were analyzed. The reproducibility of the results was checked by

using three different sets of functionalized substrates and bacterial culture batches. Each fluorescence intensity image corresponds to an average of 4 frames.

A total of 15-20 images per zoom were analyzed. On each image, the bacterial counting was performed using ImageJ image processing software. Due to the satisfying correspondence between cell counting on images obtained using zoom 1 and zoom 3 the data are pooled together. Analyses of variance (ANOVA) were performed using Statgraphics software (Manugistic, Rockville, MD). Evaluated factors were considered statistically significant when P values associated with the Fischer test were below 0.05.

Results and discussion

Surfaces preparation and characterization

A schematic representation of the three steps to construct the AMP coated surfaces is depicted in Figure 1. This process is specific for the AMP immobilization via an amine function, which is more efficient than via a carboxylic acid function (16).

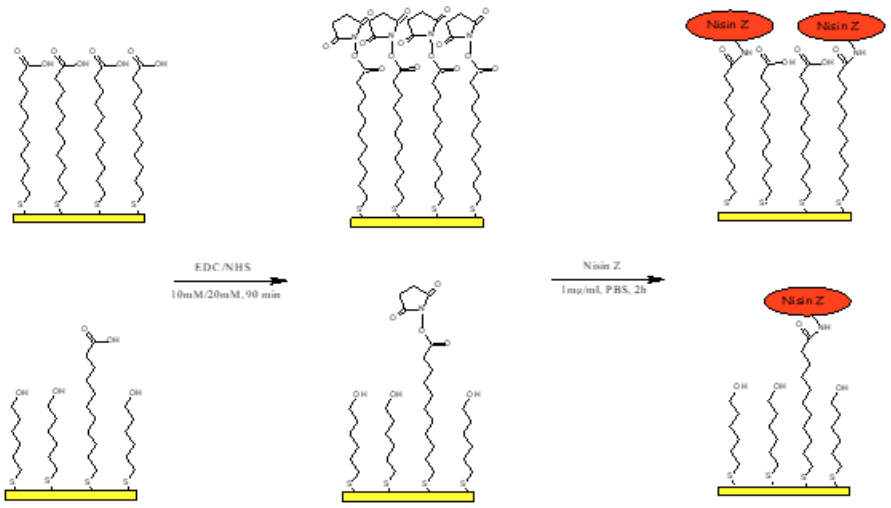

Figure 1: Schematic representation of steps involved for covalent nisin Z immobilization on gold surface. Step 1: MUA and HS(CH2)6 OH adsorption on gold surface named Au-MUA and Au-MUA25 surfaces; step 2: esterification of the COOH functionalities by NHS/EDC; step3: covalent binding of nisin Z, named Au-MUA-Nis and Au-MUA25-Nis surfaces.

The first step is the functionalization of the gold surfaces by self-assembled monolayers composed of (i) mercapoundecanoic acid or (ii) a mixture (25/75) of MUA and 6-

mercaptohexanol. The latter is expected to insert between the MUA chains, in order to limit (i) the repulsive interactions between carboxylate functions which could impact the monolayers conformation and/or (ii) residual unreacted carboxylic acid functions (with AMP) which could promote bacterial adhesion by hydrogen bonds.

The second step is the conversion of the MUA carboxylic acid functions into NHS esters by the carbodiimide chemistry allowing the AMP attachment through an amide function. The EDC and NHS concentrations were chosen in order to prevent the formation of byproducts (30).

Finally, the third step is the covalent immobilization of nisin Z on activated surfaces which occurred to preferentially select an AMP linkage with its N-terminal amide function. For this purpose, the pH was maintained at 7.4 to prevent the unwanted deprotonation of the ε-amine groups of the three lysine residues (pKa 12.2) (21). To maintain the nisin Z antibacterial effect, it is of importance that the lysine residues do not bind to the surface and remain available to interact electrostatically with bacteria.

XPS, FTIR-ATR and surface wettability were used to attest to the surface functionalization and further to the immobilization of the nisin Z peptides. All results are detailed in the supplementary information. However, XPS analysis seems to demonstrate a higher peptide immobilization on Au-MUA compared to Au-MUA25 (if we consider that all the NHS ester groups are converted). But, we never observe a four times larger effect for Au-MUA compared to Au-MUA25 substrates, suggesting that the nisin peptides could dimerize on the surface as reported (32).

SFG characterization

The SFG spectra of the different surfaces were measured both in the C-H stretching region (2700-3100 cm^{-1}) (Figure 2A) and in the amide band region (1400-1700 cm^{-1}) (Figure 2B). In this latter domain, no SFG signal was expected before peptide immobilization. It was the case for Au-MUA and Au-MUA25 samples but upon surface activation, a weak signal arised. It was ascribed to the side-reaction product N-acyl urea (identified from FTIR spectroscopy) (Supplementary information), which contains amide bonds. In the C-H stretching region, the SFG spectra of the control Au-MUA and Au-MUA25 surfaces exhibit three vibrational bands centred at 2929 cm^{-1}, 2907 cm^{-1} and 2856 cm^{-1} (Figure 2A). These frequencies are in good agreement with previous reported data (34). The 2856 and 2929 cm^{-1} bands are assigned to the symmetric and asymmetric methylene stretching modes of MUA, respectively. Several assignments of the band at 2907 cm^{-1} were reported. It may correspond to a Fermi resonance of the CH_2 groups. Another assignment was the symmetric stretching mode of the CH_2 groups at

the bottom (S-CH_2 still observed for octadecanethiol on Au (27)) or the top (CH_2-C=O) of the MUA chain. Their specific local environments may result in a different frequency than the other CH_2 groups. However, considering the SFG spectrum after activation of the surface by EDC/NHS (Figure 2A) which leads to the transformation of the acid group into the ester group without modifying S-CH_2, this band at 2907 cm^{-1} was significantly weakened. This highlighted that the contribution of CH_2-C=O at the top of the alkyl chain is larger than that of S-CH_2. It must be noted that this band at 2907 cm^{-1} is too weak to be observed in FTIR-ATR spectra, where the strong bands of the numerous CH_2 groups dominate the spectrum (Supplementary information).

The observation of these different bands confirms what has been noticed from FTIR-ATR measurements (Supplementary information), that alkyl chains of Au-MUA and Au-MUA25 surfaces are not as expected perfectly ordered both before and after activation. In such case, as mentioned above, the contribution of the CH_2 groups to the SFG spectra should vanish. This disorder of the alkyl chains may be due to steric hindrance and/or to the presence of H-bonds among terminal acid groups but also to electrostatic repulsion between these terminal groups in the case of elimination of protons during sample preparation. All are expected to distort alkyl chain conformation from all-trans.

Interestingly, the dilution of MUA into mercaptohexanol results in a clear weakening of CH_2 bands, both from Au-MUA to Au-MUA25 and from Au-MUA_{act} to Au-$MUA25_{act}$. This highlights the success of the strategy to increase the order of the MUA layer by the distance of the COOH/COO^- groups.

The attachment of the succinimidyl ester termination also results in an intensity decrease of the symmetric and asymmetric CH_2 bands (from Au-MUA to Au-MUA_{act} and from Au-MUA25 to Au-$MUA25_{act}$), which can be ascribed to a conformation of the alkyl chains closer to all trans thanks to the elimination of the interactions between COOH or COO^- groups.

A

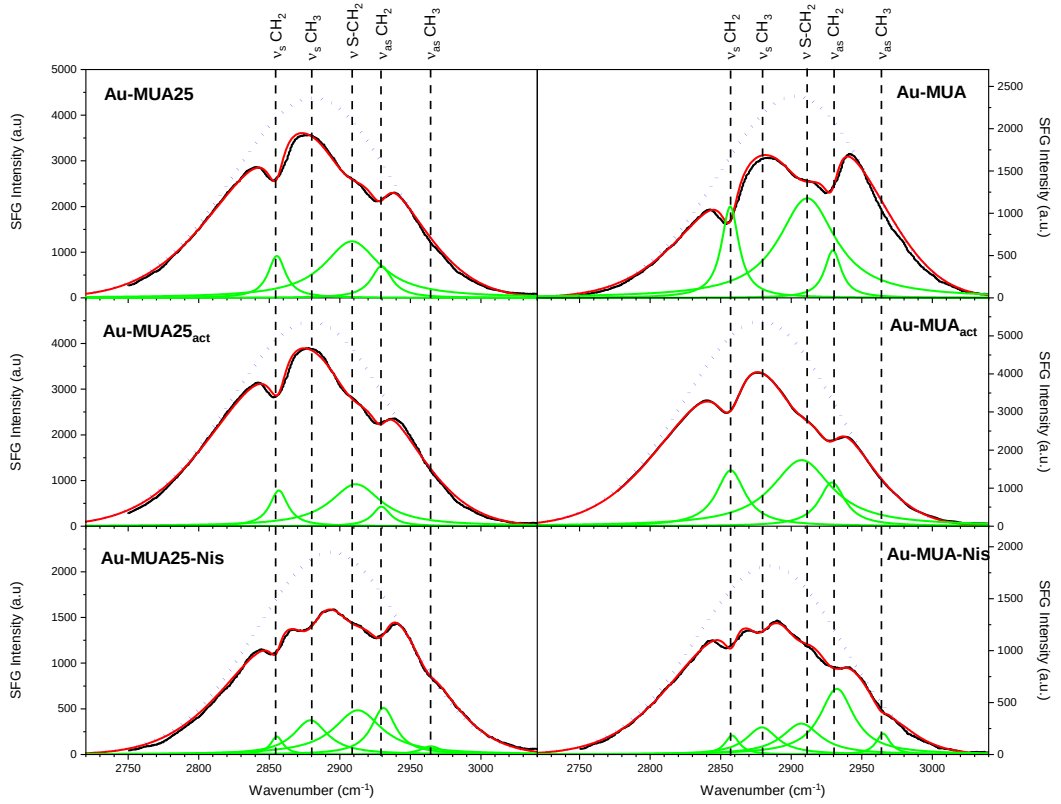
νs CH2
νs CH3
ν S-CH2
νas CH2
νas CH3
Au-MUA25
Au-MUA
Au-MUA25act
Au-MUAact
Au-MUA25-Nis
Au-MUA-Nis
SFG Intensity (a.u)
SFG Intensity (a.u.)
Wavenumber (cm-1)

B

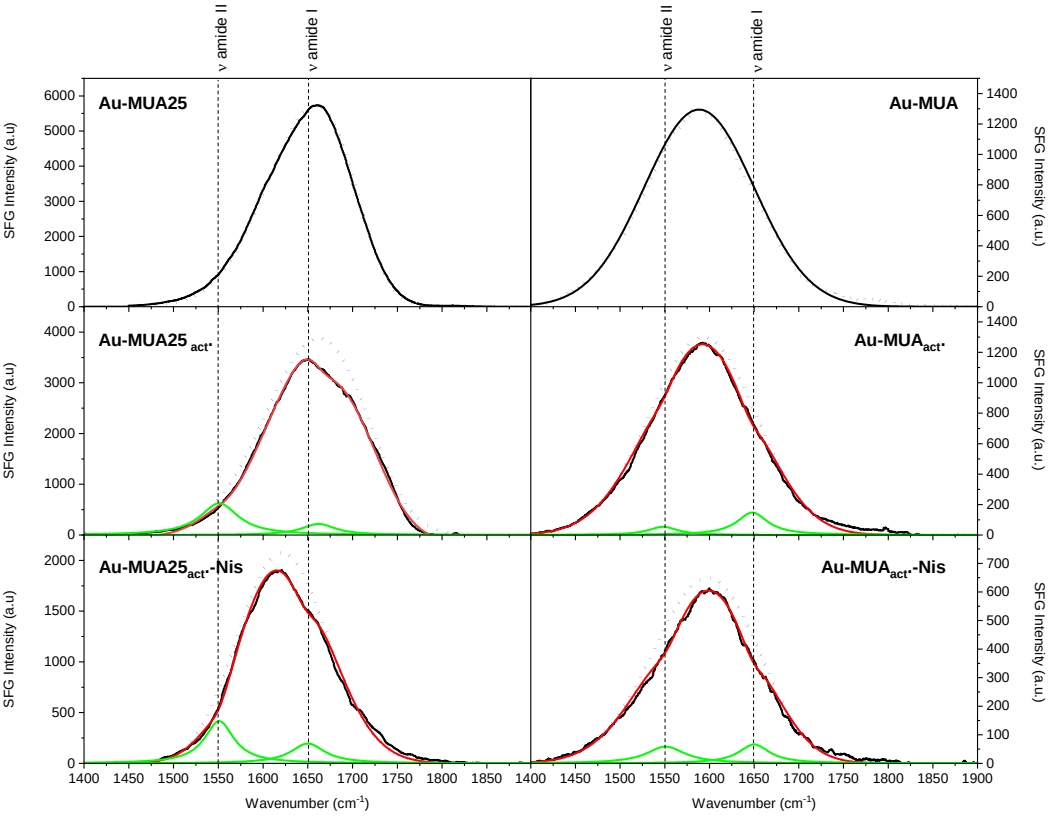
ν amide II
ν amide I
Au-MUA25
Au-MUA
Au-MUA25act•
Au-MUAact•
Au-MUA25act•-Nis
Au-MUAact•-Nis
SFG Intensity (a.u)
SFG Intensity (a.u.)
Wavenumber (cm-1)

Figure 2: SFG spectra of Au-MUA and Au-MUA25 surfaces in (A) the C-H stretching region and (B) the amide bands region. Experimental (black lines), fitted (red lines) SFG spectra, and deconvoluted vibrational bands (green lines). The SFG reference spectrum (blue dashed line) is also presented.

The binding of nisin Z was ascertain from XPS, FTIR-ATR and water-contact angle measurements as reported in Supplementary Information. It results also in three major changes in the SFG spectra: (i) the appearance of the bands corresponding to the methyl groups (19 methyl groups are present in nisin Z) at 2876 cm^{-1} and 2930 cm^{-1}corresponding the symmetric and asymmetric stretching modes, respectively. What is striking is their weak intensity relative to their large number, but it is not unexpected considering their presumably large orientation distribution in such a complex molecule (25): if it was completely isotropic, the bands would vanish completely. (ii) The reversed intensities of symmetric and asymmetric CH_2 bands with respect to the activated surfaces. Since, on metallic surfaces, dipole moments parallel to the surface plane do not contribute to SFG, and since the CH_2 asymmetric dipole moment is along the H H direction, the intensity of the asymmetric mode can be larger than the symmetric one if the CH_2 plane is not parallel to the surface and the H H direction is normal to the surface. This configuration hardly occurs in the case of an alkyl chain in a well ordered SAM. It must be related to a specific CH_2 group inside nizin Z, or to a specific modification of the alkyl chain conformation imposed by the bonding of the AMP. It can be also noted that despite the presence of additional CH_2 groups in nisin Z, no significant change of the intensity of the CH_2 bands is observed, indicating again an isotropic distribution of the dipole moments. Interpreting in more details the relative intensities of the CH bands would require in-depth density functional theory (DFT) calculations of SAM-Nis conformation on the surface, which is beyond reach of the present study. (iii) The appearance of two bands with weak intensities at ~1650 cm^{-1}, and ~1550 cm^{-1}, corresponding to amide I and amide II vibrational modes, respectively. It ascertains qualitatively the presence of amide groups on the surface. However, in this case also, quantitative analysis is impossible: nisin Z has a polycyclic structure (26) and contains 33 amide groups, so the situation is comparable with that of CH_3 modes: if the orientation distribution of the amide groups is close to being isotropic, then their SFG signature is expected to be very weak, which is the case. Additionally, the formation of nisin Z dimers on the surface, as suggested from XPS data (supplementary information), may also be responsible of this low SFG signal. Interestingly, we observe the presence of both amide I and amide II bands. Previous studies (33) have investigated by SFG the orientation of the R-helical peptide cecropin P1

(containing 31 amino acids) deposited on polymer surfaces. The selective presence of the amide I band was explained by the fact that the peptide structure contains only α helices. The selective presence of amide I was also observed for peptides with a β-sheet structure (34). By contrast, nisin Z has a polycyclic structure (26) and contains no helix. Therefore, our results suggest that the presence of both amide I and II bands is related to the polycyclic structure of nisin Z.

Antibacterial effect of nisin Z coated surfaces

Adhesion of *S. aureus* bacteria on Au-MUA and Au-MUA 25 surfaces was imaged and quantified using fluorescence confocal microscopy allowing to control the homogeneity of the surfaces.

As observed on Figure 3a, (zoom 1 and 3), the adhered cells appeared homogeneously distributed, isolated or in some groupings (a well-known behavior for *S.aureus* cells). It was previously reported that the surface topography of Au deposited on glass substrates presents platens of 1-2μm^2 separated by grooves of 20-30 nm depth (28). The *S.aureus* cells seem to adhere on these platens and not on the grooves due to their small thickness with respect to size and form of bacteria (coccoid structure of ~1µm).

If we now consider the quantification of the adhered *S. aureus* bacteria, no statistical valid difference in surface coverage was obtained for Au, Au-MUA and Au-MUA25 (Figure 3b). Neither the higher hydrophilicity of the surfaces grafted with MUA chains by comparison with a gold surface (Table 3), nor the higher charge of the Au-MUA than the Au-MUA25 surfaces via the carboxylic groups of the MUA chains have significant effect on the cell adhesion. Thus, the interactions between bacteria and the surface are rather short-distance interactions in agreement with the low number of adhered bacteria (~$5x10^6$ bacteria/ cm^2) (Figure 3b).

Assuming an average bacterium section of 1 μm^2, this corresponds to ~ 5.0 % of the bacterial surface coverage (Figure 3b). It is also interesting to note the low coverage of cells with damaged membrane and /or dead cells (in red on Figure 3a) on Au, Au-MUA and Au-MUA25 surfaces. Their quantification (~10%, Figure 3d) is comparable to what is commonly encountered in the process of bacterial adhesion. This reveals that neither the adlayer of MUA chains nor the alcohol function of 6-mercaptohexanol chains have any damaging effect on the cell membrane.

The covalent attachment of nisin Z to the Au-MUA and Au-MUA25 surfaces leads to a decrease in the number of adhered *S. aureus* after 1h30 (~ 70% for Au-MUA-Nis substrates and 95% for

Au-MUA25-Nis substrates) by comparison to the corresponding surfaces without peptides (Figure 3 b, c). Furthermore, the percentages of dead or damaged cells on the surfaces with nisin Z are higher (~20%) by comparison with Au-MUA and Au-UA25 substrates (~10%) (Figure 3d).

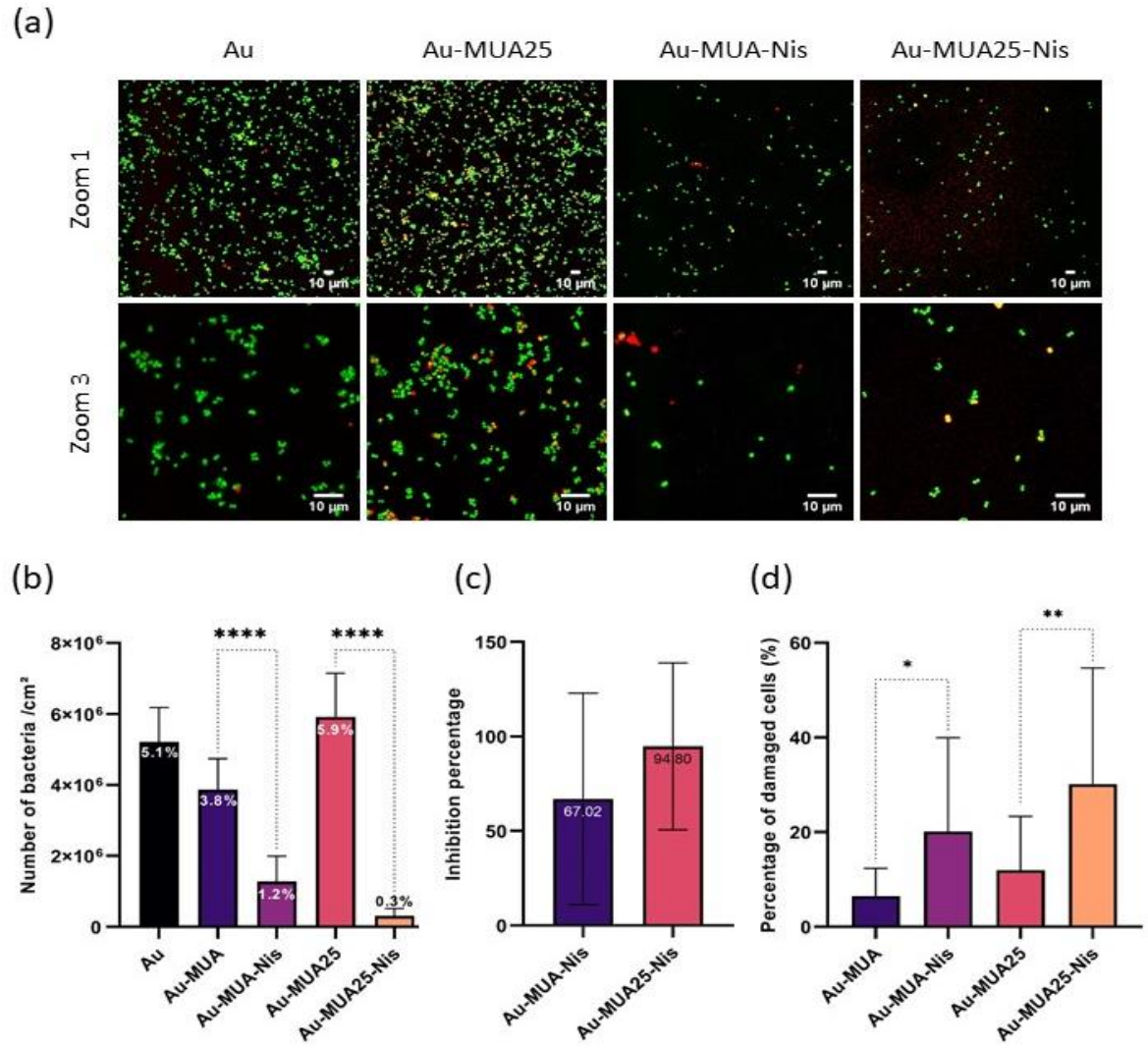

Figure 3 (a) Representative confocal fluorescence images with zooms 1 and 3, highlighting both live (green) and dead or damaged (red) S.aureus cells immobilized on different surfaces for 1h30. Bacteria were stained with Syto9/IP LIVE/DEAD staining dyes. (b) Average concentrations of adhered bacteria on the different surfaces and the corresponding average percentages of coverage (%) of the surfaces. The presented data are the average of measurements in three spots of the same surface (c) inhibition of adhesion of S.aureus on Au-MUA-Nis and Au-MUA25-Nis surfaces as compared to Au-MUA and Au-MUA25 substrates respectively. (d) Average percentages of dead or damaged cells on each surfaces

Undoubtedly, the nisin Z peptide although immobilized on a surface has a biocidal activity against *S. aureus* bacteria. As already mentioned, the mode of action of immobilized nisin Z to

kill bacteria cannot be through the “pore model” created on the cytoplasmic cell membrane, the peptide length being too short. The electrostatic interaction of nisin Z with the outer surface of bacteria is sufficient for its lethal activity. A detailed study of antimicrobial effects of positively charged surfaces on adhered Gram positive bacteria similar to *S. aureus* has shown that while bacteria are strongly attracted by the surface charges, they cannot grow (8). The interpretation is that the cell division cannot occur because the required cell elongation is prevented by the strong electrostatic interactions. Such a process can interpret our results. It is consistent with the increase of dead and/or damaged bacteria in the presence of nisin Z (Figure 3d). It tends to show that the bacteria first adhere to the surface but are then permeabilized by the grafted peptide, modifying their cell wall surface and allowing the entry of PI as observed for Magainin I on Gram positive bacteria (35). Thus on nisin Z grafted surfaces, the bacteria die "naturally" being unable to divide on the surface. Our results are also in agreement with the better efficiency when the covalent grafting of nisin Z is via its N terminal part, leaving available the lysine residues for electrostatic interaction and in particular its terminal C part, identified as the one that allows to permeabilize the target membrane (26).

The most important result proves in this study concerns the role of the order of the surface; the better order of the Au-MUA25-Nis substrate, as revealed by SFG analysis, results in a higher antibacterial effect even if higher amount of nisin Z were immobilized on Au-MUA.

Conclusion

We have developed a model of AMP surfaces by the covalent immobilization of the nisin Z peptides via its N terminal part on carboxyl functionalized gold substrate using carbodiimide coupling, the active C terminal part of the peptide being available to interact with the bacteria. Using XPS, FTIR-ATR and SFG spectroscopy and water contact angle measurements, we have verified successful surface modification after each reaction steps. Interestingly, SFG measurements allow to highlight that the conformational ordering of the Au-MUA25 substrates is significantly improved by comparison to Au-MUA substrates. Consequently, the antibacterial activity of the so-immobilized nisin Z surfaces can achieve (95%) against *S. aureus,* depending on the surface order of the attachment centers of the peptides and on the peptide orientation. These findings provide essential information for the development of antibacterial surfaces based on covalently immobilized peptides.

The whole procedure for constructing such AMP surfaces is simple, reproducible and efficient. Furthermore, the safety of antimicrobial peptides for human health has been demonstrated.

Therefore, such biocidal surfaces present great potential in packaging and industrial production surfaces (cosmetic, food, medical devices...) to avoid product contamination.

AUTHOR INFORMATION

Corresponding Author

** E-mail address: pascal.thebault@univ-rouen.fr*

ACKNOWLEDGMENT

We thank Farah Savina (ISMO, Université Paris Saclay), Ariane Deniset (ICP, Université Paris Saclay) and Julien Deschamp () for their helpful technical advice during contact angle, FTIR-ATR measurements and bacterial preparation respectively. M.A.is grateful for the financial support by the Lebanese Association for Scientific Research (LASER).

REFERENCES

1. Alvarez-Ordóñez A, Coughlan LM, Briandet R, Cotter PD. Biofilms in Food Processing Environments: Challenges and Opportunities. Annu Rev Food Sci Technol. 25 mars 2019;10(1):173-95.

2. Gupta P, Sarkar S, Das B, Bhattacharjee S, Tribedi P. Biofilm, pathogenesis and prevention—a journey to break the wall: a review. Arch Microbiol. janv 2016;198(1):1-15.

3. Levin-Reisman I, Ronin I, Gefen O, Braniss I, Shoresh N, Balaban NQ. Antibiotic tolerance facilitates the evolution of resistance. Science. 24 févr 2017;355(6327):826-30.

4. Zhang X, Wang L, Levänen E. Superhydrophobic surfaces for the reduction of bacterial adhesion. RSC Adv. 2013;3(30):12003.

5. Roy S, Das PK. Antibacterial hydrogels of amino acid-based cationic amphiphiles. Biotechnol Bioeng. 1 juill 2008;100(4):756-64.

6. Morán G, Ramos-Chagas G, Hugelier S, Xie X, Boudjemaa R, Ruckebusch C, et al. Superhydrophobic polypyrene films to prevent *Staphylococcus aureus* and *Pseudomonas aeruginosa* biofilm adhesion on surfaces: high efficiency deciphered by fluorescence microscopy. Photochem Photobiol Sci. 2018;17(8):1023-35.

7. Chappaz B. Imagerie moléculaire corrélative de nanosondes fonctionnalisées pour l'étude de l'hétérogénéité physico-chimique spatiale de microorganismes associés aux surfaces.Thesis of the university Paris-Saclay27 novem 2015.

8. Gottenbos B. Antimicrobial effects of positively charged surfaces on adhering Gram-positive and Gram-negative bacteria. J Antimicrob Chemother. 1 juill 2001;48(1):7-13.

9. Tischer M, Pradel G, Ohlsen K, Holzgrabe U. Quaternary Ammonium Salts and Their Antimicrobial Potential: Targets or Nonspecific Interactions? ChemMedChem. 2 janv 2012;7(1):22-31.

10. Alves D, Olívia Pereira M. Mini-review: Antimicrobial peptides and enzymes as promising candidates to functionalize biomaterial surfaces. Biofouling. 21 avr 2014;30(4):483-99.

11. Onaizi SA, Leong SSJ. Tethering antimicrobial peptides: Current status and potential challenges. Biotechnol Adv. janv 2011;29(1):67-74.

12. Costa F, Carvalho IF, Montelaro RC, Gomes P, Martins MCL. Covalent immobilization of antimicrobial peptides (AMPs) onto biomaterial surfaces. Acta Biomater. avr 2011;7(4):1431-40.

13. Kamra T, Chaudhary S, Xu C, Montelius L, Schnadt J, Ye L. Covalent immobilization of molecularly imprinted polymer nanoparticles on a gold surface using carbodiimide coupling for chemical sensing. J Colloid Interface Sci. janv 2016;461:1-8.

14. Vreuls C, Zocchi G, Thierry B, Garitte G, Griesser SS, Archambeau C, et al. Prevention of bacterial biofilms by covalent immobilization of peptides onto plasma polymer functionalized substrates. J Mater Chem. 2010;20(37):8092.

15. Mularski A, Wilksch JJ, Wang H, Hossain MA, Wade JD, Separovic F, et al. Atomic Force Microscopy Reveals the Mechanobiology of Lytic Peptide Action on Bacteria. Langmuir. 9 juin 2015;31(22):6164-71.

16. Paris J-B, Seyer D, Jouenne T, Thébault P. Elaboration of antibacterial plastic surfaces by a combination of antiadhesive and biocidal coatings of natural products. Colloids Surf B Biointerfaces. août 2017;156:186-93.

17. Héquet A, Humblot V, Berjeaud J-M, Pradier C-M. Optimized grafting of antimicrobial peptides on stainless steel surface and biofilm resistance tests. Colloids Surf B Biointerfaces. juin 2011;84(2):301-9.

18. Yala J-F, Thebault P, Héquet A, Humblot V, Pradier C-M, Berjeaud J-M. Elaboration of antibiofilm materials by chemical grafting of an antimicrobial peptide. Appl Microbiol Biotechnol. févr 2011;89(3):623-34.

19. Archer NK, Mazaitis MJ, Costerton JW, Leid JG, Powers ME, Shirtliff ME. *Staphylococcus aureus* biofilms: Properties, regulation, and roles in human disease. Virulence. sept 2011;2(5):445-59.

20. Guiotto A, Pozzobon M, Canevari M, Manganelli R, Scarin M, Veronese FM. PEGylation of the antimicrobial peptide nisin A: problems and perspectives. Il Farm. janv 2003;58(1):45-50.

21. Joshi PR, McGuire J, Neff JA. Synthesis and antibacterial activity of nisin-containing block copolymers. J Biomed Mater Res B Appl Biomater. oct 2009;91B(1):128-34.

22. Zendo T, Yoneyama F, Sonomoto K. Lactococcal membrane-permeabilizing antimicrobial peptides, Appl. Microbiol. Biotechnol., 2010, 88(1), 1-9.

23. Boudjemaa R, Cabriel C, Dubois-Brissonnet F, Bourg N, Dupuis G, Gruss A, et al. Impact of Bacterial Membrane Fatty Acid Composition on the Failure of Daptomycin To Kill *Staphylococcus aureus*. Antimicrob Agents Chemother. 7 mai 2018;62(7):e00023-18, /aac/62/7/e00023-18.atom.

24. Schneider N, Werkmeister K, Pischetsrieder M. Analysis of nisin A, nisin Z and their degradation products by LCMS/MS. Food Chem. juill 2011;127(2):847-54.

25. van den Hooven HW, Fogolari F, Rollema HS, Konings RNH, Hilbers CW, van de Ven FJM. NMR and circular dichroism studies of the lantibiotic nisin in non-aqueous environments. FEBS Lett. 15 mars 1993;319(1-2):189-94.

26. Rink R, Wierenga J, Kuipers A, Kluskens LD, Driessen AJM, Kuipers OP, et al. Dissection and Modulation of the Four Distinct Activities of nisin by Mutagenesis of Rings A and B and by C-Terminal Truncation. Appl Environ Microbiol. 15 sept 2007;73(18):5809-16.

27. Dykes GA, Hancock REW, Hastings JW. Structural Variations in nisin Associated with Different Membrane Mimicking and pH Environments. Biochem Biophys Res Commun. juin 1998;247(3):723-7.

28. Bulard E, Guo Z, Zheng W, Dubost H, Fontaine-Aupart M-P, Bellon-Fontaine M-N, et al. Non-Invasive Vibrational SFG Spectroscopy Reveals That Bacterial Adhesion Can Alter the Conformation of Grafted “Brush” Chains on SAM. Langmuir. 19 avr 2011;27(8):4928-35.

29. Chen X, Chen Z. SFG studies on interactions between antimicrobial peptides and supported lipid bilayers. Biochim Biophys Actai BBA - Biomembr. sept 2006;1758(9):1257-73.

30. Sam S, Touahir L, Salvador Andresa J, Allongue P, Chazalviel J-N, Gouget-Laemmel AC, et al. Semiquantitative Study of the EDC/NHS Activation of Acid Terminal Groups at Modified Porous Silicon Surfaces. Langmuir. 19 janv 2010;26(2):809-14.

31. Piard J-C, Muriana PM, Desmazeaud MJ, Klaenhammer TR. Purification and Partial Characterization of Lacticin 481, a Lanthionine-Containing Bacteriocin Produced by Lactococcus lactis subsp. lactis CNRZ 481. Appl Environ Microbiol. 1992;58(1):279-84.

32. Casford MTL, Ge A, Kett PJN, Ye S, Davies PB. The Structure of Lipid Bilayers Adsorbed on Activated Carboxy-Terminated Monolayers Investigated by Sum Frequency Generation Spectroscopy. J Phys Chem B. 27 mars 2014;118(12):3335-45.

33. Ye S, Nguyen KT, Boughton AP, Mello CM, Chen Z. Orientation Difference of Chemically Immobilized and Physically Adsorbed Biological Molecules on Polymers Detected at the Solid/Liquid Interfaces in Situ. Langmuir. 4 mai 2010;26(9):6471-7.

34. Chen X, Wang J, Sniadecki JJ, Even MA, Chen Z. Probing α-Helical and β-Sheet Structures of Peptides at Solid/Liquid Interfaces with SFG. Langmuir. mars 2005;21(7):2662-4.

35. Humblot V, Yala J-F, Thebault P, Boukerma K, Héquet A, Berjeaud J-M, et al. The antibacterial activity of Magainin I immobilized onto mixed thiols Self-Assembled Monolayers. Biomaterials. juill 2009;30(21):3503-12.

Graphical Abstract

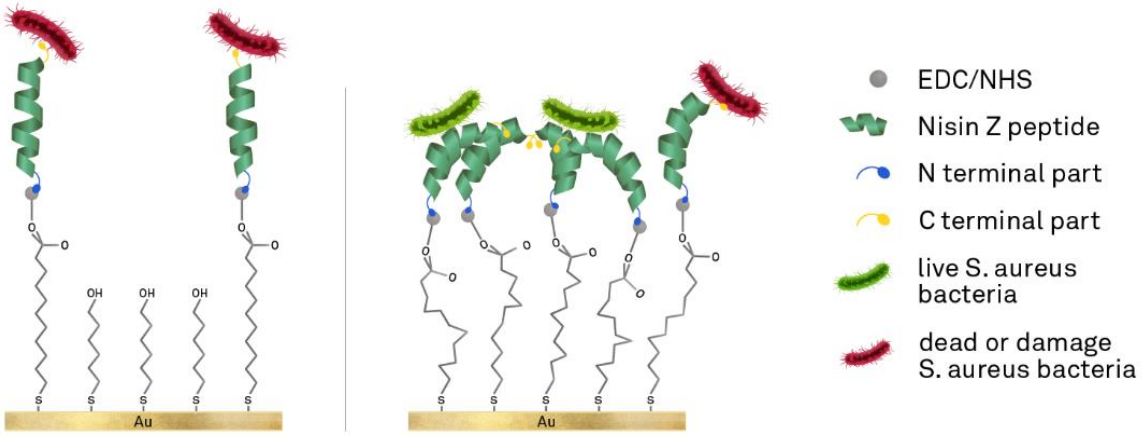

Supplementary Information

Surface characterization

XPS measurements.

XPS measurements of gold surface after MUA and MUA/$(CH_2)_6$ OH immobilization and after nisin Z binding are illustrated in Figure S1 and summarized in Table S1. The XPS spectra of unmodified gold surfaces show C1s and O1s peaks, as expected when Au surface are not prepared in ultra-high vacuum conditions (13). They are mainly due to hydrocarbon impurities (C1s peak) and to -OH from water molecules (O1s peak). Comparison of the XPS data for the gold surfaces before and after MUA functionalization, revealed the appearance of a sulfur peak and the decrease of Au4f intensity both on Au-MUA and Au-MUA25 surfaces (Table S1), confirming immobilization of thiols on the gold surfaces (13,35,S1). The attenuation of the Au4f peak by the adlayer was more important for Au-MUA corresponding to a higher thickness of MUA layer compared to MUA25 (11 carbons for MUA chain vs 6 carbons for mercaptohexanol). The high resolution analysis of the S2p peaks (Table S2, Figure S1) reveals the presence of two sulfur components, one at 162.1 eV ($S2p_{3/2}$) and 163.4 eV ($S2p_{1/2}$) attributed to sulfur atoms bound to the gold surface (in red on Figure S1) and the second one at 163.7 eV ($S2p_{3/2}$) and 164.9 eV ($S2p_{1/2}$) corresponding to free thiol functions (in blue on Figure S1) (S2). The free thiols content was larger for Au-MUA (45%) compared to Au-MUA 25 (30%). The presence of free sulfur is probably due to the formation of a partial bilayer through hydrogen bonds between the carboxylic terminal groups of thiols bonded to the surface and free thiols from the solution (in this case, the S atom outwards from the surface). This was further confirmed by IR spectra analyses (see FTIR-ATR section). The high resolution XPS spectra of the C1s region for Au-MUA and Au-MUA25 substrates (Figure S1, Table S2), were best fitted with four components corresponding to C-C/C-H bonds at 285 eV, carbon in α position of heteroatom (S and O atoms) at 286.2 eV, carboxylate functions at 288 eV and carboxylic acid functions at 289.5 eV (35,S2). Percentages of the four components were different between MUA and MUA-25 (Table S2). A lower C-S/C-O component at 286.5 eV and higher C-C/C-H and COOH contributions at 285eV and 289.5 eV, were observed for the MUA layer. These differences can be explained by the longer alkyl chain average length for MUA and the lower carboxyl group concentration for Au-MUA25.

The success of nisin Z grafting on the two types of surfaces was confirmed by (i) the significant decrease of Au4f peak intensity, (ii) the appearance of a nitrogen peak (N1s) centered at 400.2 (Table S1, Figure S1) assigned to the amide functions of the peptide (35) and (iii) an approximatively twice larger free sulfur peak after nisin Z immobilization (Figure S1) due to the presence of sulfur atoms from thioether functions in the peptide (16,17). These effects were more pronounced for Au-MUA-Nis surface by comparison to Au-MUA25-Nis.

Table S1: Surface atomic composition of gold and modified gold surfaces determined by XPS The proportion of component composition from peak areas were performed using the CasaXPS software system and applying a Gaussian/Lorentzian ratio (70/30).

Surfaces	**Atomic composition (%)**				
	Au 4f	C 1s	O 1s	S 2p	N 1s
Gold	60.4	29.4	10.2	-	-
Au-MUA	46.8	38.1	13	2.1	-
Au-MUA25	57.8	27.3	12.3	2.6	-
Au-MUA-Nis	19.8	54.2	14.3	2.2	9.5
Au-MUA25-Nis	32.2	41.8	15.5	2.5	8

Table S2: C1s and S2p chemical composition (%) of modified surfaces

	Carbon components (%)				**Sulfur components (%)**	
Surfaces	C-C/C-H (285 eV)	C-S/C-O (286.5 eV)	COO^-/ N-C=O (288 eV)	COOH (289.5 eV)	S-Au (162.1 eV)	Free S (163.7 eV)
Au-MUA	72.7	13.4	6.1	7.8	55.2	44.8
Au-MUA25	64.7	22.8	6.4	6.1	69.6	30.4
AU-MUA-Nis	59.1	23.7	15.6	1.6	28	72
Au-MUA25-Nis	56.5	26.7	15.3	1.5	45	55

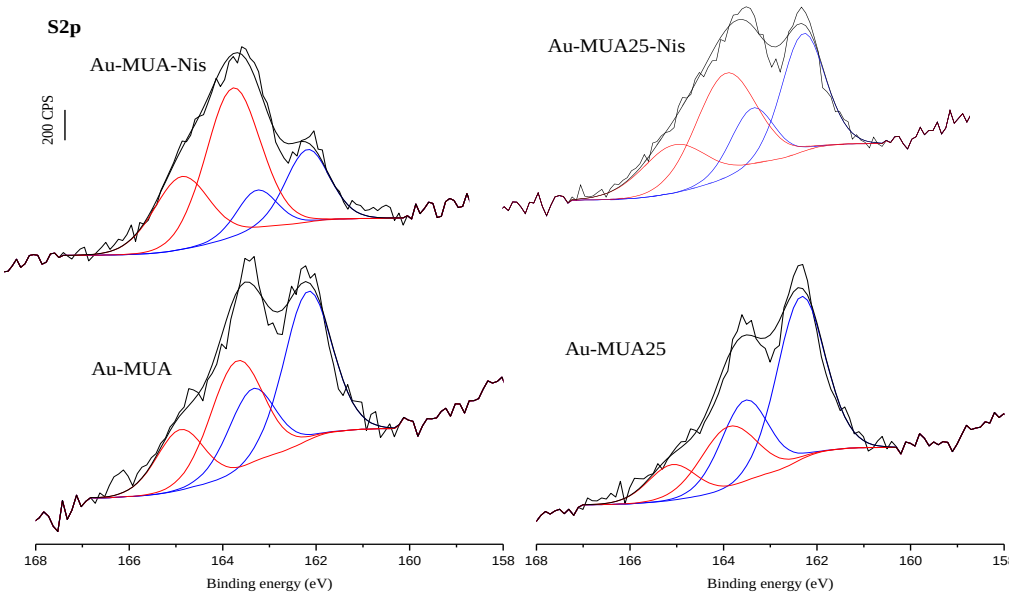
S2p
Au-MUA-Nis
200 CPS
Au-MUA25-Nis
Au-MUA
Au-MUA25
168
166
164
162
160
158
Binding energy (eV)

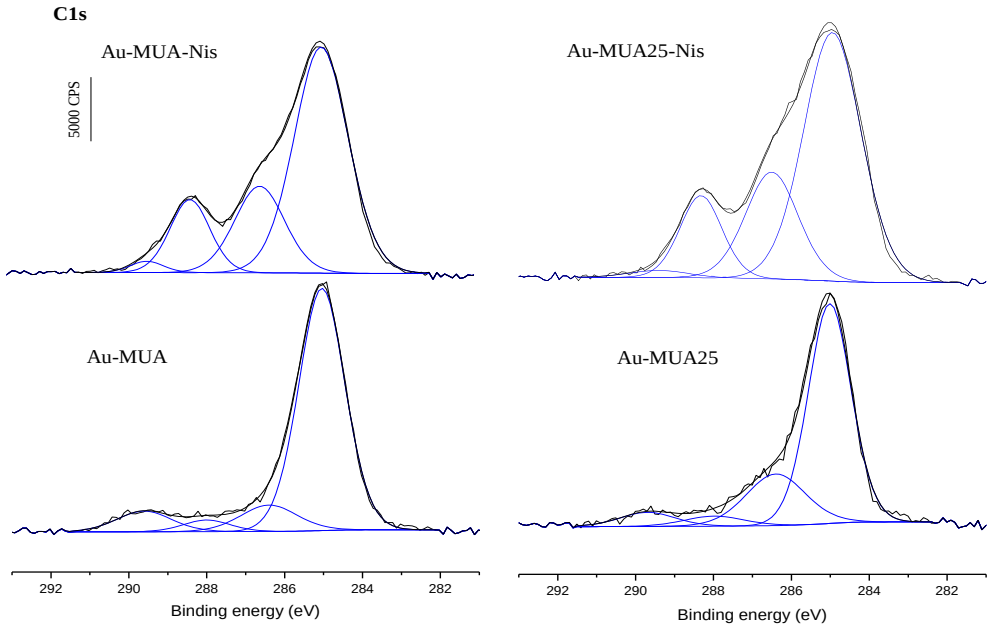
C1s
Au-MUA-Nis
5000 CPS
Au-MUA25-Nis
Au-MUA
Au-MUA25
292
290
288
286
284
282
Binding energy (eV)

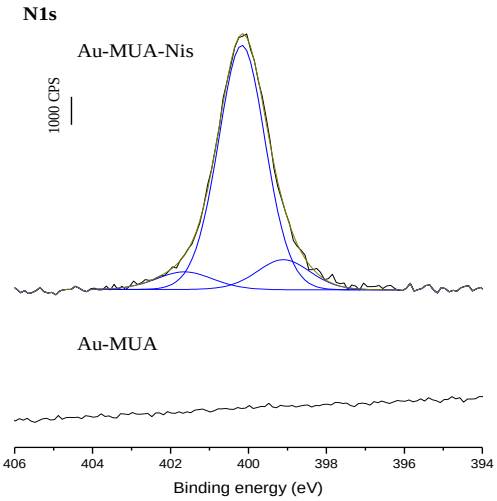
N1s
Au-MUA-Nis
1000 CPS
Au-MUA
406
404
402
400
398
396
394
Binding energy (eV)

Figure S1: High resolution XPS spectra of S2p, C1s and N1s regions before and after nisin Z immobilization. The spectra were acquired with a Thermo Electron K-Alpha Spectrometer using a monochromatic Al-K-Alpha X-ray source (1486.6 eV) with a spot size of 400 µm, a pass energy of 50 eV and through a range of -10 to 1350 eV with pass energy of 200 eV. The binding energy was referenced by setting the maximum C 1s peak at 285.0 eV. The deconvolution of peaks from the spectra was performed using the CasaXPS software system and applying a Gaussian/Lorentzian ratio (70/30)

FTIR-ATR measurements

FTIR-ATR measurements were obtained using a Brüker Vertex 70 FTIR spectrometer, equipped with an attenuated total reflection (ATR) accessory (PIKE MIRacle crystal plate diamond/ ZnSe) and a mercury cadmium telluride (MCT) detector cooled down by liquid nitrogen. 100 spectra were accumulated over the spectral region 3100 to 1400 cm^{-1} with a spectral resolution of 4 cm^{-1}. The background was recorded (average of 100 scans) on the ATR unit without any substrate pressed against the crystal.

Infrared spectroscopy measurements further confirm the chemical composition of the surfaces at each step. The FTIR-ATR spectra for Au-MUA and Au-MUA25 showed similar peak positions in the C-H stretching region, corresponding to asymmetric (2928 cm^{-1}) and symmetric (2856 cm^{-1}) stretching modes of the CH_2 alkyl chains of MUA and 6-mercaptohexanol (Figure S2). The unexpected shoulder at 2960 cm^{-1} corresponds to the asymmetric band of the methyl group. It was due to impurities related to MUA conditioning as revealed by the spectrum of a KBr pellet of MUA, where it is present (S1). The corresponding symmetric band of this methyl group is expected at ≈2880 cm^{-1}. It is not clearly visible, presumably because it is weaker than its asymmetric counterpart and is hidden in the wings of other bands. The frequency of the asymmetric methylene stretching is reported to be sensitive to conformational ordering: the more ordered the alkyl chain, the lower the frequency (2918 cm^{-1} for a well-ordered alkyl chain) (S3). Therefore, the position of the asymmetric band of Au-MUA and Au-MUA25 before and after activation at 2928 cm^{-1} suggests a certain disorder of the thiol layers. This was supported by the IR spectra measured in the frequency range 1800 cm^{-1}-1500 cm^{-1}. Figure S2). The two bands at 1742 cm^{-1} and 1714 cm^{-1} were attributed to the CO stretching mode of non-hydrogen-bonded and hydrogen-bonded carboxylic acid groups, respectively (32,35). The band at 1714 cm^{-1} is consistent with the ability of carboxylic acids to undergo strong intermolecular hydrogen bounding interaction. This can occur from head to head MUA chain dimers forming a partial bilayer of MUA chains, as already suggested from XPS data. Nevertheless, dimerization of

carboxylic groups of neighboring MUA chains may also exist, which would imply disorder within the layer. Elsewhere, the large absorption signals in the range 1570-1540 cm^{-1} and the band at 1463 cm^{-1} are ascribed to the asymmetric and symmetric stretching modes of COO^- respectively. It reveals that some deprotonated COO^- groups are present. They are able to induce electrostatic repulsion and presumably a relative disorder of the surface layer (S4). SFG measurements further support this disorder of the Au-MUA and Au-MUA25 layers.

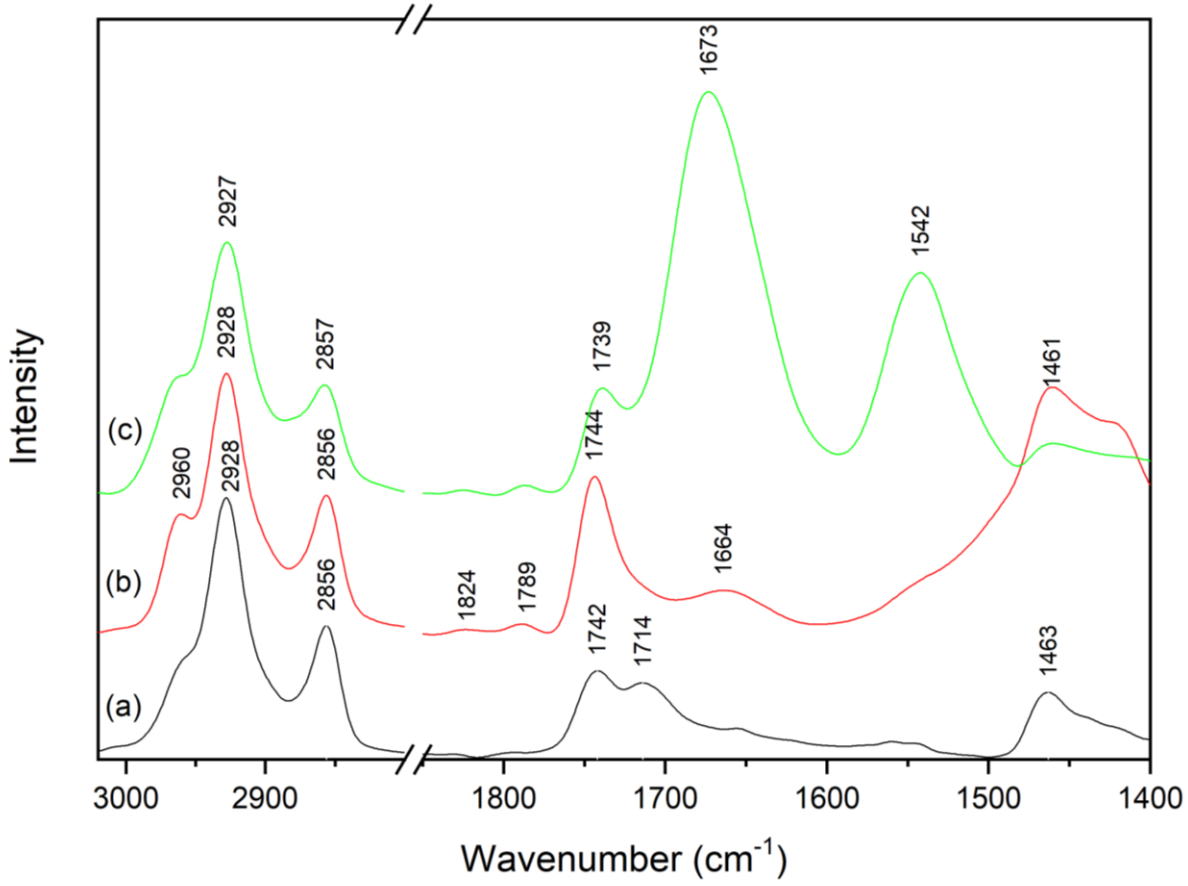

Figure S2: FTTR-ATR spectra of the three consecutive steps leading to the nisin Z immobilization: (a) Au-MUA or Au-MUA25, (b) Au-MUA$_{act}$ or Au-MUA25$_{act}$ by NHS/EDC, (c) covalent binding of Nisin Z, Au-MUA-Nis or Au-MUA25-Nis.

At the second step of surface preparation (termination by the succinimidyl ester), two more CH_2 groups (present in the succinimidyl cycle) are added on each MUA chain. However, their contribution to the CH_2 symmetric and asymmetric bands does not produce a quantitative change of relative intensities (Figure S2). By contrast, this attachment of the succinimidyl ester termination is evidenced by the triplet in the spectral range of the C=O stretching vibrations: (i) the persistence of the prominent peak at 1744 cm^{-1} corresponding to the transformation of the acid terminal group into ester, (ii) the appearance of two weak bands at 1788 cm^{-1} and 1820 cm^{-1} , the signature of the ester groups of the imide ring (30,25,S5) (Figure S2). The disappearance

of the 1714 cm^{-1} absorption band highlights that the activation leads to the disruption of intermolecular hydrogen bonds between carboxylic groups. Smaller broad bands observed in some experiments at 1656 cm^{-1} and ~1550 cm^{-1} (not visible in the spectra of Figure S2), evocative of amide I and amide II bands, respectively, can be ascribed to the limited formation of the stable N-acyl urea byproduct due to defects in the activated layer (30). Finally, the broad band extending between 1500 cm^{-1} and 1400 cm^{-1} corresponds to bending modes of the different CH bonds. It cannot be exploited because it shows no structure.

Although the nisin Z peptide has an appreciable number of CH, CH_2 and CH_3 groups in various positions with respect to amide groups, the CH stretching spectrum does not show any significant change (Figure S2). However, the nisin Z grafting is ascertained by the appearance of the two strong bands at 1673 cm^{-1} and 1542 cm^{-1} that can be ascribed to the amide I and amide II bands of the peptidic backbone. In addition, a band centered at ~1739 cm^{-1} is still present. It may correspond to the free carboxylic group of the C-terminated part of Nisin and/or from remaining non-activated carboxylic groups.

Water contact angle measurements

Static water contact angle measurements of all samples were performed using a sessile drop technique with deionized water as a probe liquid. The instrument used was DSA 30S Krüss contact angle system goniometer. To check surface uniformity and reproducibility, six measurements were acquired on each of two different samples by depositing six droplets (2.5 µl milliQ water) at different points of the surface (11mm x 11mm).

Table 3 summarizes the changes in the water contact angles when moving from Au to functionalized substrates. In each case, the water contact angle values were constant over the entire sample surface demonstrating that the successive functionalization of the gold surfaces were homogeneous.

Table S3: contact angle measurements

Surfaces	Water contact angle (±1.5°)
Gold	86
Au-MUA	52
Au-MUA25	45
Au-MUA$_{act}$	61
Au-MUA25$_{act}$	51
Au-MUA-Nis	62
Au-MUA25-Nis	60

When the gold surface was modified by MUA, an increase of the surface hydrophilicity is observed due to the introduction of polar head groups (COOH) and the hydrophilicity of the mixed OH/COOH terminated surface (Au-MUA25) is higher than that of a COOH terminated surface (Au-MUA), which is consistent with the literature (12,S2). Upon EDC/NHS activation, the water contact angle increased by ~7-10°, indicating lower hydrophobicity of the surface due to the formation of the succinimide ester intermediate (13,S5). The nisin Z immobilization rendered the surfaces slightly less hydrophilic, as expected considering the amphiphilic nature of the peptide. No difference between Au-MUA and Au-MUA25 substrates was observed.

REFERENCES

S1. de la Llave E, Herrera SE, Adam C, Méndez De Leo LP, Calvo EJ, Williams FJ. Molecular and electronic structure of osmium complexes confined to Au(111) surfaces using a self-assembled molecular bridge. J Chem Phys. 14 nov 2015;143(18):184703.

S2. Mendoza SM, Arfaoui I, Zanarini S, Paolucci F, Rudolf P. Improvements in the Characterization of the Crystalline Structure of Acid-Terminated Alkanethiol Self-Assembled Monolayers on Au(111). Langmuir. janv 2007;23(2):582-8.

S3. Nuzzo RG, Dubois LH, Allara DL. Fundamental studies of microscopic wetting on organic surfaces. 1. Formation and structural characterization of a self-consistent series of polyfunctional organic monolayers. J Am Chem Soc. janv 1990;112(2):558-69.

S4. Methivier C, Beccard B, Pradier CM. In Situ Analysis of a Mercaptoundecanoic Acid Layer on Gold in Liquid Phase, by PM-IRAS. Evidence for Chemical Changes with the Solvent. :6.

S5. Afara N, Omanovic S, Asghari-Khiavi M. Functionalization of a gold surface with fibronectin (FN) covalently bound to mixed alkanethiol self-assembled monolayers (SAMs): The influence of SAM composition on its physicochemical properties and FN surface secondary structure. Thin Solid Films. nov 2012;522:381-9.